ACS OMEGA

http://pubs.acs.org/journal/acsodf

Article

Indium-Doped Rutile Titanium Oxide with Reduced Particle Length and Its Sodium Storage Properties

Hiroyuki Usui, Yasuhiro Domi, Thi Hay Nguyen, Yuri Tanaka, and Hiroki Sakaguchi*

Cite This: *ACS Omega* 2020, 5, 15495−15501

Read Online

ACCESS | Metrics & More | Article Recommendations | Supporting Information

ABSTRACT: We hydrothermally synthesized In-doped rutile TiO_2 particles in an anionic surfactant solution and investigated the influences of In doping and the particle morphology on the Na^+ storage properties. The solid solubility limit was found to be 0.8 atom % in In-doped TiO_2. In the case where no surfactant was used, the best anode performance was obtained for 0.8 atom % In-doped TiO_2 electrode by the benefits of three doping effects: (i) expanded diffusion-path size, (ii) improved electronic conductivity, and (iii) reduced electron charge density in the path. Further enhancement in the performance was achieved for the In-doped TiO_2 with a reduced particle length by the synthesis in the surfactant solution. This electrode exhibited a better cycle stability and maintained a high discharge capacity of 240 mA h g^{-1} for 200 cycles. The reason is probably that Na^+ can be inserted in the inner part of TiO_2 particles because of its reduced particle length.

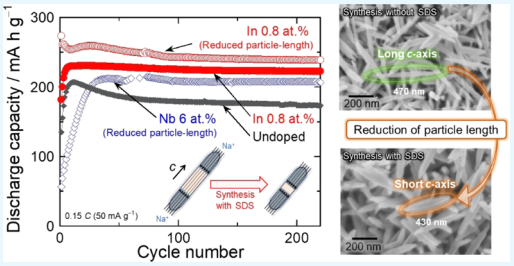

1. INTRODUCTION

Na-ion batteries (NIBs) have extensively attracted research interest because of the easy availability and low cost of Na resources since Braconnier and Delmas et al. first reported a promising cathode material, $NaCoO_2$, in 1980.[1] The charge−discharge mechanism of NIBs is based on a rocking-chair mechanism system, which is the same as that of Li-ion batteries (LIBs). Thus, replacing Li^+ with Na^+ was effective for developing electrode materials and electrolytes. In particular, great progress has been achieved in developing promising cathode materials composed of rare-metal-free and low-cost elements, $NaFeO_2$,[2] $Na_x[Fe_{1/2}Mn_{1/2}]O_2$,[3] and $Na_2Fe_2(SO_4)_3$.[4] On the other hand, graphite anodes in LIBs cannot be used for NIBs because Na^+ cannot be electrochemically intercalated into a graphite structure owing to its larger ionic size compared to Li^+.[5]

Titanium-based compounds are prospective candidates as NIB anode materials because Ti^{4+}/Ti^{3+} redox reactions occur at lower electrode potentials compared with other transition-metal-based compounds. Among them, titanium oxides are the most desirable from the viewpoint of abundance, cost-effectiveness, and nontoxicity.[6] Since 2011, many researchers have intensively studied various titanium oxide-based materials such as $Na_2Ti_3O_7$,[7] $NaTi_2(PO_4)_3$,[8] bronze-type TiO_2,[9] $Na_2Ti_3O_7$,[10] $Na_{2+x}Ti_6O_{13}$,[11] anatase-type TiO_2,[12,13] and $Na_3LiTi_5O_{12}$.[14]

Rutile-type TiO_2 had never drawn attention from any of the researchers since the authors first reported it in 2015 and even in numerous studies because it had been well known that rutile TiO_2 shows much less Li activity as an LIB anode owing to two reasons. (i) One reason is its highly anisotropic ion-diffusion path along the *c*-axis direction. Rutile TiO_2 originally has a unique diffusion path capable of high-speed Li^+ conduction with an extremely high diffusion coefficient of 10^{-6} cm^2 s^{-1} along the *c*-axis direction, which is attributed to the very low electron charge density in the diffusion path.[15] Thus, Li^+ can easily diffuse in a single crystal of rutile TiO_2 along its *c*-axis direction. However, Li^+ diffusion is strongly restricted in polycrystalline rutile TiO_2 particles with many grain boundaries because of its very low diffusion coefficient of 10^{-14} cm^2 s^{-1} along the *ab* in-plane direction. (ii) The other reason is its poor electronic conductivity. The intrinsic electrical resistivity of rutile TiO_2 is as high as 10^{13} Ω·cm, which impedes the progress of the electrochemical reaction.

To address the above issues, the authors have adopted two kinds of approaches: the doping of impurity elements into the crystal structure[16] and the improvement of the crystallinity of TiO_2 particles.[17] These approaches could improve the electronic conductivity and the trapping at grain boundaries, leading to a remarkable enhancement in the Li^+ storage performances. It is noteworthy that the anode of highly crystalline Nb-doped TiO_2 exhibited a faster charge−discharge performance than the $Li_4Ti_5O_{12}$ anode in practical use.[17] Consequently, we conceived that these two approaches would be effective for NIB also and carried out those. As a result, the authors revealed in 2015 that the Nb-doped TiO_2 anode

Received: April 8, 2020
Accepted: June 3, 2020
Published: June 16, 2020

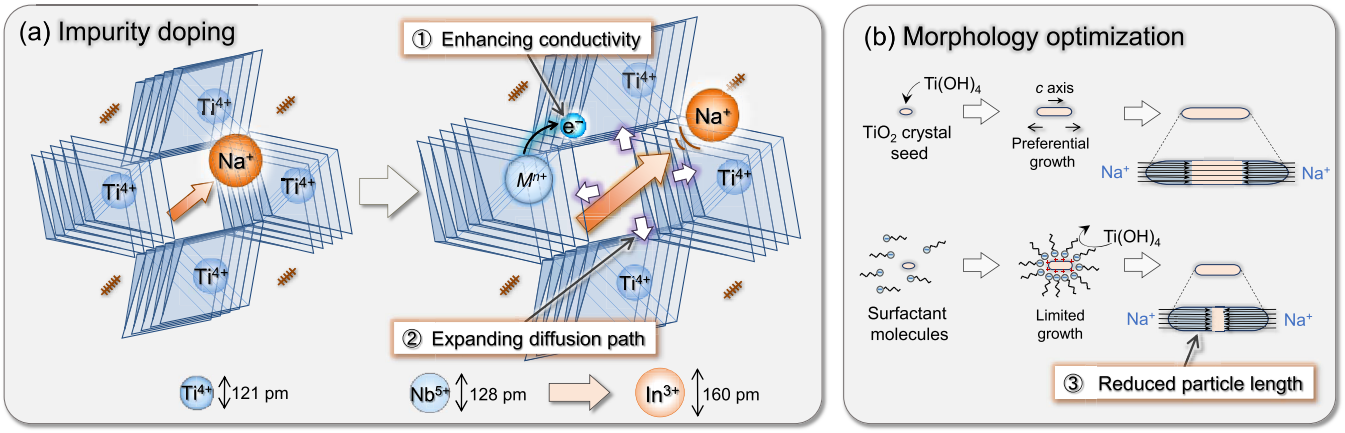

Figure 1. Two strategies used in this study to improve the anode performances of rutile TiO_2. (a) Impurity-element doping enhances the electronic conductivity and expands the size of the diffusion path along its *c*-axis direction. (b) Morphology optimization of TiO_2 particles by synthesis in an anionic surfactant solution. TiO_2 preferentially grows along its *c*-axis, which is an unfavorable morphology for Na^+ insertion into the inner part. Surfactant molecules limit the growth to shorten the particle length.

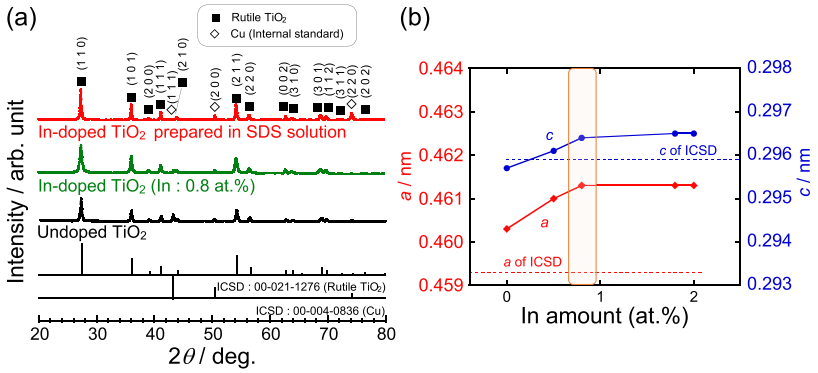

Figure 2. (a) XRD patterns of 0.8 atom % In-doped TiO_2 prepared in solutions with and without the sodium dodecyl sulfate (SDS) surfactant. (b) Lattice parameters *a* and *c* of In-doped TiO_2 with various In amounts.

clearly showed improved performance,[16] which was the first study to report the reversible charge−discharge reactions of rutile-type TiO_2. After the first report, Zhang[18] and He et al.[19−21] reported the improved Na-storage properties of rutile TiO_2. Due to these developments, rutile TiO_2 has gradually gained much attention as a potential NIB anode material. For further enhancement in the performance, the authors hydrothermally synthesized single-crystalline rutile TiO_2 particles,[22] and have performed the doping of various impurity elements (Ta, Sn, and In) other than Nb.[23] A high reversible capacity of 200 mA h g^{-1} was achieved even after a long period of 800 cycles by the electrodes prepared using single-crystalline particles of Nb-doped TiO_2[22] and Ta-doped TiO_2[23] (Figure S1). These results demonstrated that the formation of single-crystalline particles and the impurity-element doping are very effective for improving the insertion−extraction properties of Na^+. Nevertheless, there still remains a serious problem that the capacity steeply increases or decreases in the initial several tens of cycles even by Nb doping and Ta doping.

The doping of Nb and Ta has another effect of expanding the crystal lattice of rutile TiO_2 because the sites of Ti^{4+} (ionic diameter: 121 pm) are substituted with Nb^{5+} (128 pm) and Ta^{5+} (128 pm). This expansion is accompanied by an increase in the size of Na^+ diffusion path, which is favorable for improving the insertion−extraction properties of Na^+. Since the ionic diameter of Na^+ (204 pm) is larger than that of Li^+ (152 pm), the size expansion of the ion-diffusion path is more important for NIB compared with LIB.

Indium (In) has a much larger ionic size of 160 pm than Nb and Ta. It is thus expected that the larger size will change the doping effects on Na^+'s insertion−extraction properties. In the previous study,[23] the authors did not systematically investigate the dependence of In doping amount on the anode properties. Therefore, in this study, we evaluated the anode properties of In-doped rutile electrodes with various doping amounts to clarify the influence of In doping (Figure 1a).

Another problem exists with single-crystalline rutile TiO_2 particles obtained by the hydrothermal synthesis: the large aspect ratio of the particles. Although glycolic acid is a key material in the solution of the hydrothermal reaction to produce single-crystalline particles, it cannot avoid generating large aspect-ratio particles.[24] Unfortunately, its longer axis is parallel to the *c*-axis direction of the rutile crystal. This is disadvantageous for Na^+ insertion and extraction because Na^+ cannot be stored in the inner part of the particles. Owing to such problems, the author had previously succeeded in controlling some oxides' morphologies using anionic surfactant molecules in various solution-based syntheses such as laser ablation in solution, precipitation synthesis, and electrodeposition.[25−29] In the hydrothermal synthesis also, the anionic surfactant solution could successfully reduce the particle length of the longer axis, leading to the increase in

https://dx.doi.org/10.1021/acsomega.0c01623
ACS Omega 2020, 5, 15495−15501

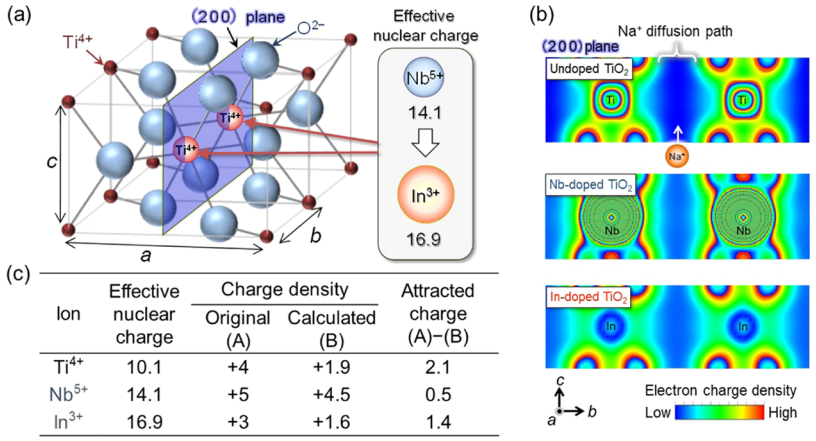

(c)

Ion	Effective nuclear charge	Charge density		Attracted charge (A)−(B)
		Original (A)	Calculated (B)	
Ti^{4+}	10.1	+4	+1.9	2.1
Nb^{5+}	14.1	+5	+4.5	0.5
In^{3+}	16.9	+3	+1.6	1.4

Figure 3. (a) Calculation system of an In-doped rutile TiO_2 crystal. Ti^{4+} at the center of the unit cell was substituted by In^{3+}. (b) Calculation results of the electron charge density mapping. Na^+ diffuses in the diffusion path along the *c*-axis. (c) Electron charge densities attracted by impurity ions. When this value is larger, the diffusion path has lower electron charge to promote an easier Na^+ diffusion.

the reversible capacity of Nb-doped TiO_2 electrodes.[22] As another strategy to improve the performance, in this study we tried to reduce the particle length of single-crystalline In-doped TiO_2 using anionic surfactant molecules in the hydrothermal synthesis (Figure 1b).

2. RESULTS AND DISCUSSION

Figure 2a shows X-ray diffraction (XRD) patterns of the synthesized powders of undoped TiO_2 and 0.8 atom % In-doped TiO_2. The resulting patterns were in good agreement with the rutile phase (Inorganic Crystal Structure Database, ICSD No. 00-021-1276). The crystallite size was estimated to be 35−40 nm using the Scherrer equation and the full width at half-maximum of the diffraction peaks.

Figure 2b represents the lattice parameters *a* and *c* for In-doped TiO_2 with various In amounts. In the range of the indium amount from 0 to 0.8 atom %, the lattice parameters were linearly increased according to Vegard's law, indicating a substitutional solid solution of In^{3+} with a larger ionic size of 160 pm compared to that of Ti^{4+} (121 pm). The solid solubility limit of In in rutile TiO_2 was approximately 0.8 atom %. A sample of 2.0 atom % In-doped TiO_2 also showed XRD peaks of only rutile TiO_2 (Figure S2). However, it should contain some amorphous-like impurities such as In_2O_3 because the doping amount of 2.0 atom % exceeded enough the solid solubility limit of 0.8 atom %. The lattice parameter *a* is more important than *c* because it determines the cross-sectional size of the Na^+ diffusion path along the *c*-axis direction. The lattice parameter *a* increased from 0.4603 to 0.4613 nm by 0.8 atom % In doping. This size expansion of the diffusion path contributes to the easier Na^+ diffusion in rutile TiO_2. The degree of size expansion by In doping is comparable to the change from 0.4603 to 0.4619 nm by 6 atom % of Nb doping. The remarkable feature is that a similar increase in size can be achieved even with a much smaller doping amount in the case of In doping because of its larger ionic size.

To maintain the charge balance, it is suggested that the actual composition of In-doped TiO_2 would be $(Ti^{4+})_{1-x}(In^{3+})_x(O^{2-})_{2-(x/2)}$ by the generation of oxygen defects.[30] Such oxygen-deficient In-doped TiO_2 has been reported to behave as an n-type semiconductor.[31] It is thus expected that the electronic conductivity is increased by the doped In and the oxygen defects. Electrical resistivity measurements of the powder pressed under 60 MPa revealed that 0.8 atom % In-doped TiO_2 has an electronic conductivity of 1.5×10^{-1} S cm^{-1}, which is 10 times higher than that of undoped TiO_2 (1.3×10^{-2} S cm^{-1}). A similar improvement in the conductivity was obtained for 6 atom % Nb-doped TiO_2. We should here note that In doping could improve the conductivity in spite of its much less doping amount than Nb.

These results demonstrated that In doping delivered two effects desirable for the Na^+ storage: the size expansion of the diffusion path and the improvement in the electronic conductivity. Recently, the authors have newly discovered the third effect for rutile TiO_2: the reduction of the electron charge density in the diffusion path.[23] Rutile TiO_2 intrinsically has a low electron charge density in its diffusion path along the *c*-axis direction, enabling a significantly smooth diffusion of Li^+.[15] Consequently, we have suggested a new approach: the reduction of the charge density by an impurity doping. In the previous study,[23] when Ta^{5+} was doped into rutile, the charge density could be reduced because Ta^{5+} has a larger effective nuclear charge of 20.5 for its outermost electron than Ti^{4+} (10.5) and Nb^{5+} (14.1). The reduced charge density resulted in improved anode performance. In^{3+} also has a relatively large effective nuclear charge of 16.9. As shown in Figure 3a, the electron charge density of the diffusion path in In-doped TiO_2 was calculated by the first-principle calculation. The diffusion path of undoped TiO_2 shows a dark blue color, indicating a very low electron charge density (Figure 3b). In the case of Nb doping, the color of the diffusion path was confirmed to be light blue.[23] In contrast, it became dark blue when In was doped. Indium has originally a positive charge of +3 by ionization in a polar crystal. The positive charge is actually weakened by attracting the surrounding electrons according to the degree of its effective nuclear charge. The actual charge density of In^{3+} can be calculated using the Bader method.[26,27] The actual charge density of In^{3+} was 1.6, indicating that the charge of 1.4 in the surrounding electrons was attracted by In^{3+}. The attracted charge of In^{3+} was obviously larger than that of Nb^{5+} (Figure 3c). This is an important evidence that In^{3+} can attract more electrons in the diffusion path because of its larger effective nuclear charge than Nb^{5+}.

Figure 4 compares the charge−discharge curves of In-doped TiO_2 electrodes cycled in an electrolyte of 1.0 dm^{-3} (M) sodium bis(fluorosulfonyl)amide (NaFSA)-dissolved/propy-

https://dx.doi.org/10.1021/acsomega.0c01623
ACS Omega 2020, 5, 15495−15501

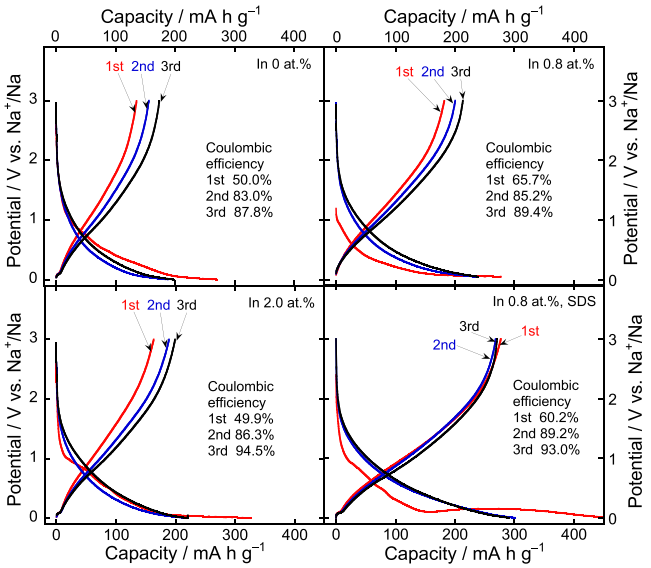

Figure 4. Charge−discharge curves of In-doped TiO_2 electrodes cycled in NaFSA/PC under 50 mA g^{-1} (0.15C) at 30 °C.

lene carbonate (PC) under a constant current density of 50 mA g^{-1} (0.15C) at 30 °C. In previous studies,[16,22,23] the authors reported that rutile TiO_2 shows gentle potential shoulders in the potential ranges of 0−1.5 and 0.2−2.0 V vs Na^+/Na during Na^+ insertion (sodiation) and Na^+ extraction (desodiation), respectively. The sodiation reactions are accompanied by a reversible 2.4% expansion in the volume of the rutile TiO_2 lattice.[16] In this study also, similar charge−discharge curve profiles were recognized for all of the electrodes, suggesting a reversible Na^+-insertion reaction in the rutile TiO_2 crystal lattice. In the cases of undoped TiO_2 and the In-doped one with In amounts of 0.8 and 2.0 atom % prepared without an SDS surfactant, the discharge (Na^+ extraction) capacities were gradually increased in the initial three cycles. This feature has also been observed for Nb-doped rutile TiO_2 (Figure S1). The gradual increase in the capacity is presumably attributed to an incomplete Na^+ extraction during the desodiation process: some Na^+ are not completely extracted in the discharge process and remain inside particles. This change would enhance the electronic conductivity and allow easier Na^+ diffusion in the particles, which improves the charge−discharge performance by repeating Na^+ insertion and extraction reactions.[22] Contrary to this, no gradual increase was observed for the electrode of 0.8 atom % In-doped TiO_2 synthesized in the SDS surfactant solution. The initial charge (Na^+ insertion) capacity was increased from 277 to 460 mA h g^{-1} by adding the surfactant. This significant increase in the capacity is probably attributed to the side reaction by the residual surfactant on the In-doped TiO_2 particles because this capacity exceeds the theoretical capacity of 335 mA h g^{-1}. The second charge capacity was reduced to 300 mA h g^{-1}, indicating that the side reaction finished in the first charge−discharge cycle. This electrode attained the highest initial discharge (Na^+ extraction) capacity of 273 mA h g^{-1}. The achievement ratio of the theoretical capacity (335 mA h g^{-1}) is as high as 81%. There was a long potential plateau at 0.1 V vs Na^+/Na in the charge process of the initial cycle, which is possibly caused by the side reaction of the residual surfactant or by an easier Na^+ insertion into TiO_2.

The initial Coulombic efficiencies of 50−65% were relatively low. He et al. have well summarized the reasons for the initial irreversible capacity of various NIB anode materials.[32] Based on the author's summary, there are three main reasons for the TiO_2 anode: (i) the electrolyte decomposition and the resulting formation of a solid-electrolyte interphase, (ii) crystal defects, and (iii) the trap effect of Na^+. The authors have previously applied an ionic liquid electrolyte to rutile TiO_2 electrodes for suppressing the electrolyte decomposition.[33] However, the initial Coulombic efficiency did not improve even by applying the ionic liquid electrolyte. The crystal defects are not the main reason in this study because hydrothermal synthesis can produce single-crystalline TiO_2 particles. In addition to this, the Coulombic efficiencies were low irrespective of whether In was doped or not. It is, therefore, suggested that the main reason is possibly the trap effect of Na^+ in the TiO_2 crystal lattice. Compared to TiO_2 as an LIB anode, the trap effect would be more pronounced for TiO_2 as an NIB anode owing to the larger ionic size of Na^+ than Li^+. To improve this effect, we suggest the dual doping of a cation (In^{3+}) and anions such as F^-, Cl^-, S^{2-}, and N^{3-}. Since the dual dopings will increase the solid solubility limit of In^{3+}, the Na^+-diffusion path can be further expanded to suppress the trap effect of Na^+. In future work, the authors would like to investigate the dual doping.

Figure 5a presents the cycling performances of these In-doped TiO_2 electrodes. When SDS was not used in the

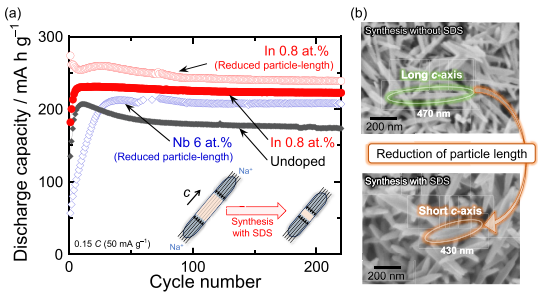

Figure 5. (a) Cycling performances of electrodes prepared using 0.8 atom % In-doped TiO_2 particles. When the particles were prepared in the SDS surfactant solution, the particle length was reduced. For comparison, the figure shows the performance of an electrode of 6 atom % Nb-doped TiO_2 particles prepared in a 0.1 M SDS solution. (b) SEM images of 0.8 atom % In-doped TiO_2 particles.

synthesis, the 0.8 atom % In-doped TiO_2 electrode exhibited a very constant discharge capacity of 220 mA h g^{-1} after a gradual increase in the initial five cycles. This capacity was higher than that of 170 mA h g^{-1} obtained for the undoped one at the 200th cycle. The enhanced capacity is due to the benefit of the three kinds of doping effects:[23] the diffusion-path size expansion, the improved electronic conductivity, and the reduced electron charge density in the path. The performance of the 2.0 atom % In-doped TiO_2 electrode was, however, inferior to that of the 0.8 atom % In-doped TiO_2 one (Figure S4). The reason is probably the Na-inactive impurity phase generated by exceeding the solid solubility limit. On the other hand, a further enhancement in the performance was attained for the In-doped TiO_2 synthesized using the SDS surfactant. A high capacity of 240 mA h g^{-1} was maintained even after 200 cycles. The mechanism is suggested to be an improved utilization rate of TiO_2: Na^+ can be inserted in the inner part of TiO_2 particles because of its reduced particle length along the

https://dx.doi.org/10.1021/acsomega.0c01623
ACS Omega 2020, 5, 15495−15501

c-axis. To verify the mechanism, the particle morphology was observed. Figure 5b displays scanning electron microscopic (SEM) images of these In-doped TiO_2 particles. A rod-like morphology was confirmed. This shape has been commonly observed for single-crystalline rutile TiO_2 prepared by hydrothermal methods.[22−24] The average particle length was successfully decreased from 470 to 440 nm by the addition of 0.1 M SDS surfactant in the synthesis. An approximately 7% reduction in the particle length (from 470 to 440 nm) caused a 9% increase in the discharge capacity (from 220 to 240 mA h g^{-1}). Although the rate of length reduction is low, the particle-length reduction is very effective because a previous study has reported that a reduction rate of 58% (from 400 to 170 nm) resulted in only 15% increase in the capacity (from 170 to 200 mA h g^{-1}) for Nb-doped TiO_2.[22] The pH value of the glycolic acid solution was about 3.0 in the hydrothermal synthesis. A TiO_2 particle has a positive surface charge because its isoelectric point is 6.0. It is suggested that anionic surfactant molecules were attached on the positively charged TiO_2 surface during the crystal growth, having the effect that the preferential growth in the *c*-axis direction was relatively suppressed.[18] As the author has previously reported, the SDS surfactant can strongly affect the morphology of oxide materials in the particle formation.[25−29] Thus, we expected a shorter particle length at higher SDS concentration. However, at a higher concentration of 0.5 M SDS, the performance was not improved owing to the presence of residual surfactant in the samples (Figure S4). To further reduce the particle length, we should optimize not the SDS concentration but the glycolic acid concentration,[24] which will be done in our future works. In this study, we consider that the optimal SDS concentration is 0.1 M because the best performance was achieved at this concentration. In addition, a notable advantage of the In-doped TiO_2 electrode is its good cyclability. The capacities were considerably decreased or increased during the initial 10 cycles in the case of Nb-doped TiO_2[22] and Ta-doped TiO_2[23] (Figure S1). Such considerable change in the capacity was greatly improved by the In doping and the reduced particle length in this study. This result is a very valuable evidence showing the potential high performance of rutile-type TiO_2 with a unique diffusion path along the *c*-axis.

3. CONCLUSIONS

As NIB anode materials, In-doped rutile TiO_2 particles were synthesized by the hydrothermal method using an anionic surfactant solution. XRD analyses for various In doping amounts revealed that the solid solubility limit of In was approximately 0.8 atom % for TiO_2. In the case where no surfactant was used, the best anode performance was obtained for the 0.8 atom % In-doped TiO_2 electrode because of the benefits of the three doping effects: (i) the diffusion-path size expansion, (ii) the improved electronic conductivity, and (iii) the reduced electron charge density in the path. Further enhancement in the performance was achieved for the 0.8 atom % In-doped TiO_2 electrode using the surfactant in the synthesis. The surfactant could reduce the particle length from 470 to 440 nm. This electrode exhibited a better cycle stability and maintained a high discharge capacity of 240 mA h g^{-1} for 200 cycles. The reason is probably that Na^+ can be inserted in the inner part of TiO_2 particles because of its reduced particle length.

4. EXPERIMENTAL SECTION

4.1. Sample Preparation. In-doped rutile TiO_2 particles were prepared by the hydrothermal synthesis using indium(III) ethoxide $In(C_2H_5O)_3$ (purity: 99.9%), titanium tetraisopropoxide ($Ti[OCH(CH_3)_2]_4$, 95.0%), isopropanol (99.5%), and glycolic acid ($HOCH_2CO_2H$, 99.0%). The detailed synthesis procedure has been reported recently.[22,23] Briefly, 0.05−0.15 g of indium(III) ethoxide, 5.0 mL of titanium tetraisopropoxide, and 5.0 mL of isopropanol were added to 50 mL of an aqueous solution of glycolic acid at a concentration of 1.6 mol dm^{-3} (M) (Figure S3). When the particle length of In-doped TiO_2 was reduced, 0.144 g of sodium dodecyl sulfate (SDS, $C_{12}H_{25}SO_4Na$, 95%) was also added into the solution. We have recently reported that SDS can reduce the Nb-doped TiO_2 particle length along its *c*-axis from 400 to 170 nm, and that its NIB anode property was improved because of easier Na^+ diffusion into the center part of the particle.[22] In the cases of SDS 0.01 and 0.5 M, the performances of In-doped TiO_2 electrodes could not be improved (Figure S4). Thus, in this study, the SDS concentration was fixed to be 0.1 M. The solution was first stirred at 80 °C for 1.5 h. Then, it was heated at 200 °C for 9−15 h in a Teflon-lined stainless steel autoclave (HU-50, SAN-AI Kagaku) using a rotation-type hydrothermal synthesis system (RDV-TM2, SAN-AI Kagaku) to promote a hydrothermal reaction. The estimated pressure in the autoclave was 1.6 MPa. After cooling, the solution obtained was washed with ethanol and dried to obtain In-doped TiO_2 particles.

4.2. Characterization. The crystal structure of the samples was confirmed by analysis using X-ray diffraction (XRD, Ultima IV, Rigaku). As shown in Figure S2, all of the samples were found to have a single phase of rutile-type TiO_2 (Inorganic Crystal Structure Database, ICSD No. 00-021-1276). The lattice parameters (a = 0.4612 nm, c = 0.2462 nm) of In-doped TiO_2 prepared with an SDS surfactant were almost equivalent to those (a = 0.4613 nm, c = 0.2464 nm) prepared without SDS. In addition, the crystallite size of 42 nm was also almost the same as that of 40 nm. The morphologies were observed by a field-emission scanning electron microscope (FE-SEM, JSM-6701F, JEOL Ltd.). The amount of doped In was detected using an energy-dispersive X-ray fluorescence (XRF) spectrometer (EDX-720 Shimadzu Co. Ltd.).

4.3. First-Principle Calculation. To discuss Na^+ behavior in the diffusion path of doped rutile TiO_2, we investigated the electron charge density using a first-principle calculation based on the density functional theory.[23] This calculation was carried out using the projector augmented wave method as implemented in the plane wave code of the Vienna Ab initio Simulation Package (VASP).[34] The charge densities of doped elements were also calculated by the Bader analysis.[35,36] A generalized gradient approximation (GGA) was used as the term exchange correlation with a kinetic energy cutoff of 350 eV. Brillouin zone sampling was performed with an 8 × 8 × 8 k point mesh within a γ point centered mesh scheme. Other detailed conditions were explained in our previous study.[37,38] Mapping figures of the electron charge density were created using the VESTA package.[39]

4.4. Charge−Discharge Test. Galvanostatic charge−discharge tests were carried out for film electrodes prepared using In-doped TiO_2 particles, acetylene black, carboxymethyl cellulose, and styrene-butadiene rubber with a weight ratio of 70:15:10:5 wt %. The active material loading was approximately 1.0 mg cm^{-2}. We assembled 2032-type coin cells

https://dx.doi.org/10.1021/acsomega.0c01623
ACS Omega 2020, 5, 15495−15501

composed of the In-doped TiO_2 electrodes, Na metal sheets, and an electrolyte of 1.0 M sodium bis(fluorosulfonyl)amide (NaFSA)-dissolved/propylene carbonate. The cycling performances were evaluated by charge−discharge tests with a potential range of 0.005−3.0 V vs Na^+/Na at 303 K at 50 mA g^{-1} (0.15C).

■ ASSOCIATED CONTENT

Supporting Information

The Supporting Information is available free of charge at https://pubs.acs.org/doi/10.1021/acsomega.0c01623.

Cycling performances, XRD patterns, schematic illustration of the hydrothermal synthesis, Coulombic efficiency (PDF)

■ AUTHOR INFORMATION

Corresponding Author

Hiroki Sakaguchi − *Department of Chemistry and Biotechnology, Graduate School of Engineering and Center for Research on Green Sustainable Chemistry, Tottori University, Tottori 680-8552, Japan;* orcid.org/0000-0002-4125-7182; Phone: +81-857-31-5265; Email: sakaguch@tottori-u.ac.jp

Authors

Hiroyuki Usui − *Department of Chemistry and Biotechnology, Graduate School of Engineering and Center for Research on Green Sustainable Chemistry, Tottori University, Tottori 680-8552, Japan;* orcid.org/0000-0002-1156-0340

Yasuhiro Domi − *Department of Chemistry and Biotechnology, Graduate School of Engineering and Center for Research on Green Sustainable Chemistry, Tottori University, Tottori 680-8552, Japan*

Thi Hay Nguyen − *Course of Chemistry and Biotechnology, Department of Engineering, Graduate School of Sustainability Science and Center for Research on Green Sustainable Chemistry, Tottori University, Tottori 680-8552, Japan*

Yuri Tanaka − *Course of Chemistry and Biotechnology, Department of Engineering, Graduate School of Sustainability Science and Center for Research on Green Sustainable Chemistry, Tottori University, Tottori 680-8552, Japan*

Complete contact information is available at: https://pubs.acs.org/10.1021/acsomega.0c01623

Notes

The authors declare no competing financial interest.

■ ACKNOWLEDGMENTS

This study was partially supported by the Japan Society for the Promotion of Science (JSPS) KAKENHI (grant numbers 19H02817, 19K05649, and 20H00399). A part of this work was supported by the Japan Association for Chemical Innovation (JACI). The authors appreciate K. Takama for his assistance in the first-principle calculation.

■ REFERENCES

(1) Braconnier, J.-J.; Delmas, C.; Fouassier, C.; Hagenmuller, P. Comportement Electrochimique Des Phases Na_xCoO_2. *Mater. Res. Bull.* **1980**, *15*, 1797−1804.

(2) Zhao, J.; Zaho, L.; Dimon, N.; Okada, S.; Nishida, T. Electrochemical and Thermal Properties of α-$NaFeO_2$ Cathode for Na-Ion Batteries. *J. Electrochem. Soc.* **2013**, *160*, A3077−A3081.

(3) Yabuuchi, N.; Iwatate, J.; Nishikawa, H.; Hitomi, S.; Okuyama, R.; Usui, R.; Yamada, Y.; Komaba, S. P2-type $Na_x[Fe_{1/2}Mn_{1/2}]O_2$ Made from Earth-Abundant Elements for Rechargeable Na Batteries. *Nat. Mater.* **2012**, *11*, 512−517.

(4) Barpanda, P.; Oyama, G.; Nishimura, S.; Chung, S.-C.; Yamada, A. A 3.8-V Earth-Abundant Sodium Battery Electrode. *Nat. Commun.* **2014**, *5*, No. 4358.

(5) Wen, Y.; He, K.; Zhu, Y.; Han, F.; Xu, Y.; Matsuda, I.; Ishii, Y.; Cumings, J.; Wang, C. Expanded Graphite as Superior Anode for Sodium-Ion Batteries. *Nat. Commun.* **2014**, *5*, No. 4033.

(6) Mei, Y.; Huang, Y.; Hu, X. Nanostructured Ti-Based Anode Materials for Na-Ion Batteries. *J. Mater. Chem. A* **2016**, *4*, 12001−12013.

(7) Senguttuvan, P.; Rousse, G.; Seznec, V.; Tarascon, J.-M.; Palacín, M. R. $Na_2Ti_3O_7$: Lowest Voltage Ever Reported Oxide Insertion Electrode for Sodium Ion Batteries. *Chem. Mater.* **2011**, *23*, 4109−4111.

(8) Park, S. I.; Gocheva, I.; Okada, S.; Yamaki, J. Electrochemical Properties of $NaTi_2(PO_4)_3$ Anode for Rechargeable Aqueous Sodium-Ion Batteries. *J. Electrochem. Soc.* **2011**, *158*, A1067−A1070.

(9) Huang, J. P.; Yuan, D. D.; Zhang, H. Z.; Cao, Y. L.; Li, G. R.; Yang, H. X.; Gao, X. P. Electrochemical Sodium Storage of TiO_2(B) Nanotubes for Sodium Ion Batteries. *RSC Adv.* **2013**, *3*, 12593−12603.

(10) Rudola, A.; Saravanan, K.; Devaraj, S.; Gong, H.; Balaya, P. $Na_2Ti_6O_{13}$: a Potential Anode for Grid-Storage Sodium-Ion Batteries. *Chem. Commun.* **2013**, *49*, 7451−7453.

(11) Shen, K.; Wagemaker, M. $Na_{2+x}Ti_6O_{13}$ as Potential Negative Electrode Material for Na-Ion Batteries. *Inorg. Chem.* **2014**, *53*, 8250−8256.

(12) Xu, Y.; Lotfabad, E. M.; Wang, H. L.; Farbod, B.; Xu, Z. W.; Kohandehghan, A.; Mitlin, D. Nanocrystalline Anatase TiO_2: a New Anode Material for Rechargeable Sodium Ion Batteries. *Chem. Commun.* **2013**, *49*, 8973−8975.

(13) Kim, K.-T.; Ali, G.; Chung, K. Y.; Yoon, C. S.; Yashiro, H.; Sun, Y.-K.; Lu, J.; Amine, K.; Myung, S.-T. Anatase Titania Nanorods as an Intercalation Anode Material for Rechargeable Sodium Batteries. *Nano Lett.* **2014**, *14*, 416−422.

(14) Kitta, M.; Kataoka, R.; Tanaka, S.; Takeichi, N.; Kohyama, M. Spinel-Type Sodium Titanium Oxide: A Promising Sodium-Insertion Material of Sodium-Ion Batteries. *ACS Appl. Energy Mater.* **2019**, *2*, 4345−4353.

(15) Steele, J. L.; MacCartney, E. R. Anisotropy of Diffusion in Rutile. *Nature* **1969**, *222*, No. 79.

(16) Usui, H.; Yoshioka, S.; Wasada, K.; Shimizu, M.; Sakaguchi, H. Nb-Doped Rutile TiO_2: a Potential Anode Material for Na-Ion Battery. *ACS Appl. Mater. Interfaces* **2015**, *7*, 6567−6573.

(17) Usui, H.; Domi, Y.; Yoshioka, S.; Kojima, K.; Sakaguchi, H. Electrochemical Lithiation and Sodiation of Nb-Doped Rutile TiO_2. *ACS Sustainable Chem. Eng.* **2016**, *4*, 6695−6702.

(18) Zhang, Y.; Foster, C. W.; Banks, C. E.; Shao, L.; Hou, H.; Zou, G.; Chen, J.; Huang, Z.; Ji, X. Graphene-Rich Wrapped Petal-Like Rutile TiO_2 tuned by Carbon Dots for High-Performance Sodium Storage. *Adv. Mater.* **2016**, *28*, 9391−9399.

(19) He, H.; Wang, H.; Sun, D.; Shao, M.; Huang, X.; Tang, Y. N-doped Rutile TiO_2/C with Significantly Enhanced Na Storage Capacity for Na-Ion Batteries. *Electrochim. Acta* **2017**, *236*, 43−52.

(20) He, H.; Sun, D.; Zhang, Q.; Fu, F.; Tang, Y.; Guo, J.; Shao, M.; Wang, H. Iron-Doped Cauliflower-Like Rutile TiO_2 with Superior Sodium Storage Properties. *ACS Appl. Mater. Interfaces* **2017**, *9*, 6093−6103.

(21) He, H.; Gan, Q.; Wang, H.; Xu, G.-L.; Zhang, X.; Huang, D.; Fu, F.; Tang, Y.; Amine, K.; Shao, M. Structure-Dependent Performance of TiO_2/C as Anode Material for Na-Ion Batteries. *Nano Energy* **2018**, *44*, 217−227.

(22) Usui, H.; Domi, Y.; Ohnishi, S.; Sakaguchi, H. Single-Crystalline Nb-Doped Rutile TiO_2 Nanoparticles as Anode Materials for Na-Ion Batteries. *ACS Appl. Nano Mater.* **2019**, *2*, 5360−5364.

(23) Usui, H.; Domi, Y.; Takama, K.; Tanaka, Y.; Sakaguchi, H. Tantalum-Doped Titanium Oxide with Rutile Structure as a Novel Anode Material for Sodium-Ion Battery. *ACS Appl. Energy Mater.* **2019**, *2*, 3056−3060.
(24) Kobayashi, M.; Petrykin, V.; Kakihana, M.; Tomiya, K. Hydrothermal Synthesis and Photocatalytic Activity of Whisker-Like Rutile-Type Titanium Dioxide. *J. Am. Ceram. Soc.* **2009**, *92*, S21−S26.
(25) Usui, H.; Shimizu, Y.; Sasaki, T.; Koshizaki, N. Photoluminescence of ZnO Nanoparticles Prepared by Pulsed Laser Ablation in Different Surfactant Solutions. *J. Phys. Chem. B* **2005**, *109*, 120−124.
(26) Usui, H. Influence of Surfactant Micelles on Morphology and Photoluminescence of Zinc Oxide Nanorods Prepared by One-Step Chemical Synthesis in Aqueous Solution. *J. Phys. Chem. C* **2007**, *111*, 9060−9095.
(27) Usui, H. The Effect of Surfactants on The Morphology and Optical Properties of Precipitated Wurtzite ZnO. *Mater. Lett.* **2009**, *63*, 1489−1492.
(28) Usui, H. Surfactant Concentration Dependence of Structure and Photocatalytic Property of Zinc Oxide Rods Prepared Using Chemical Synthesis in Aqueous Solutions. *J. Colloid Interface Sci.* **2009**, *336*, 667−674.
(29) Usui, H. Electrochemical Self-Assembly Synthesis of Zinc Oxide Nanoparticles and Lamellar-Structured Organic/Inorganic Hybrids by Electrodeposition in Surfactant Solution. *Eletrochim. Acta* **2011**, *56*, 3934−3940.
(30) Kumaravel, V.; Rhatigan, S.; Mathew, S.; Bartlett, J.; Nolan, M.; Hinder, S. J.; Sharma, P. K.; Singh, A.; Byrne, J. A.; Harrison, J.; Pillai, S. C. Indium-Doped TiO_2 Photocatalysts with High-Temperature Anatase Stability. *J. Phys. Chem. C* **2019**, *123*, 21083−21096.
(31) Nowotny, J.; Malik, A.; Alim, M. A.; Bak, T.; Atanacio, A. J. Electrical Properties and Defect Chemistry of Indium-Doped TiO_2: Electrical Conductivity. *ECS J. Solid State Sci. Technol.* **2014**, *3*, P330−P339.
(32) He, H.; Sun, D.; Tang, Y.; Wang, H.; Shao, M. Understanding and Improving the Initial Coulombic Efficiency of High-Capacity Anode Materials for Practical Sodium Ion Batteries. *Energy Storage Mater.* **2019**, *23*, 233−251.
(33) Usui, H.; Domi, Y.; Shimizu, M.; Imoto, A.; Yamaguchi, K.; Sakaguchi, H. Niobium-Doped Titanium Oxide Anode and Ionic Liquid Electrolyte for a Safe Sodium-Ion Battery. *J. Power Sources* **2016**, *329*, 428−431.
(34) Kresse, G.; Furthmüller, J. Efficient Iterative Schemes for ab initio Total-Energy Calculations Using a Plane-Wave Basis Set. *Phys. Rev. B* **1996**, *54*, 11169−11186.
(35) Henkelman, G.; Arnaldsson, A.; Jónsson, H. A Fast and Robust Algorithm for Bader Decomposition of Charge Density. *Comput. Mater. Sci.* **2006**, *36*, 354−360.
(36) Tang, W.; Sanville, E.; Henkelman, G. A Grid-Based Bader Analysis Algorithm without Lattice Bias. *J. Phys.: Condens. Matter.* **2009**, *21*, No. 084204.
(37) Usui, H.; Nouno, K.; Takemoto, Y.; Nakada, K.; Ishii, A.; Sakaguchi, H. Influence of mechanical grinding on lithium insertion and extraction properties of iron silicide/silicon composites. *J. Power Sources* **2014**, *268*, 848−852.
(38) Domi, Y.; Usui, H.; Takemoto, Y.; Yamaguchi, K.; Sakaguchi, H. Improved Electrochemical Performance of Lanthanum Silicide/Silicon Composite Electrode with Nickel Substitution for Lithium-Ion Batteries. *J. Phys. Chem. C* **2016**, *120*, 16333−16339.
(39) Momma, K.; Izumi, F. VESTA 3 for three-dimensional visualization of crystal, volumetric and morphology data. *J. Appl. Crystallogr.* **2011**, *44*, 1272−1276.

https://dx.doi.org/10.1021/acsomega.0c01623
ACS Omega 2020, 5, 15495−15501